Reducing Bubble Size Detached from Thin-wall Needles Submerged in Liquids with Pulsating Gas Flows

James Q. Feng
OXCBO Research
Maple Grove, Minnesota, 55369, USA
james.q.feng@gmail.com

ABSTRACT

The present work explores the feasibility of generating axisymmetric sub-millimeter bubbles with pulsating gas flows from thin-wall needles submerged in liquids through numerical simulations using an OpenFOAM® volume-of-fluid solver. The results for needles of inner diameters D from 0.05 to 1 mm suggest that bubbles of diameters d less than 2 D can be produced with sufficient pulse amplitude, i.e., bubbles of d < 0.1 mm may be obtained with needles of D ~ 0.05 mm, especially for liquids of relatively low viscosity. An investigation of the numerically simulated effects of liquid viscosity and surface tension reveals that the normalized bubble size d / D (regarded here as the minimum feasible value under given conditions) depends primarily on Reynolds number (Re) and Weber number (We). For example, to obtain d / D < 2 appears to require Re > 1000 while We is above a threshold value, with the feasibility window shrinking when D is reduced. Hence, using smaller needles for generating smaller bubbles could encounter more stringent requirements. As expected, liquids with a smaller contact angle (e.g., < 45°) on the needle wall are more desirable for generating smaller bubbles. Moreover, using the pulsating gas flow is likely to enable well-controlled operations with reasonable gas throughput while repeatably generating microbubbles. It can also facilitate various types of bubble-on-demand applications.

Keywords: *bubble size, submerged needle, pulsating gas flow, free surface, volume-of-fluid*

1. Introduction

Many phase-contacting applications (such as bubble columns, sparger reactors, extraction equipment, water treatment, etc.) involve bubbles generated by flowing a gas through an upward-facing orifice into a liquid tank. However, it has been found that simply using a steady constant gas flow is difficult to produce small bubbles (e.g., those of diameters less than a couple of millimeters) even with the orifice diameters much less than 1 mm, especially when attempting to increase the throughput as often practically desired [1-3]. As revealed from experiments and theoretical analyses, bubbles detached from submerged orifices or needles increase in size with the steady constant gas flowrate, even in the quasi-static regime with diminishing gas flowrate [3]. Thus, operating simply with a constant gas flow often faces a compromise between bubble size and gas throughput for a given orifice size.

Interestingly, some experimental evidence suggested the possibility of using pulsating gas flow to generate much smaller bubbles than those with a steady constant gas flow [4-8]. But in-depth understanding of the underlying mechanisms in such situations based on rigorous modeling has been lacking in the literature (e.g., there has been little beyond some lumped-parameter model calculations [7-9]).

Theoretically, the bubble formation process is governed by the Navier-Stokes equations with an appropriate description of the fluid interface motion and other boundary conditions. Although mathematically solving such a complicated partial differential system can be quite challenging, a well-established volume-of-fluid (VOF) numerical computational code available in an open-source package OpenFOAM® has

been illustrated to be effective for rigorously simulating the dynamical bubble formation process [3]. Hence, the present work would extend the recent computational study of bubble formation for constant gas flow [3] to the situation of pulsating gas flow. To avoid the complication of detached bubble size enlargement due to the three-phase contact motion outside the orifice horizontal wall [10], the propensity of which is found stronger with reducing the orifice size [3], a thin-wall needle instead of an orifice in a horizontal wall is considered here.

In what follows, section 2 concisely describes the computational model setup, with computational results for a set of case studies presented in section 3. Finally, section 4 provides concluding remarks, highlighting the significant findings of the present work.

2. Computational Model

Considered here is a pulsating gas flow through an inlet tube connected to an upward-pointing needle into a liquid tank, as shown in Fig. 1a. The needle has an outlet orifice of diameter D with a wall thickness of D / 8 (consistently throughout the present study). As described by Feng [3], the two-phase fluid flow problem is assumed axisymmetric, enabling the use of a wedge-type mesh (Fig. 1b) generated with the OpenFOAM® meshing utilities such as blockMesh, mergeMeshes, and stitchMesh for combining fine and coarse mesh patches to reduce computational burden while the free surface location can be adequately resolved (as verified with mesh refinement tests [3] and consistent with the findings of Ohta et al. [11]).

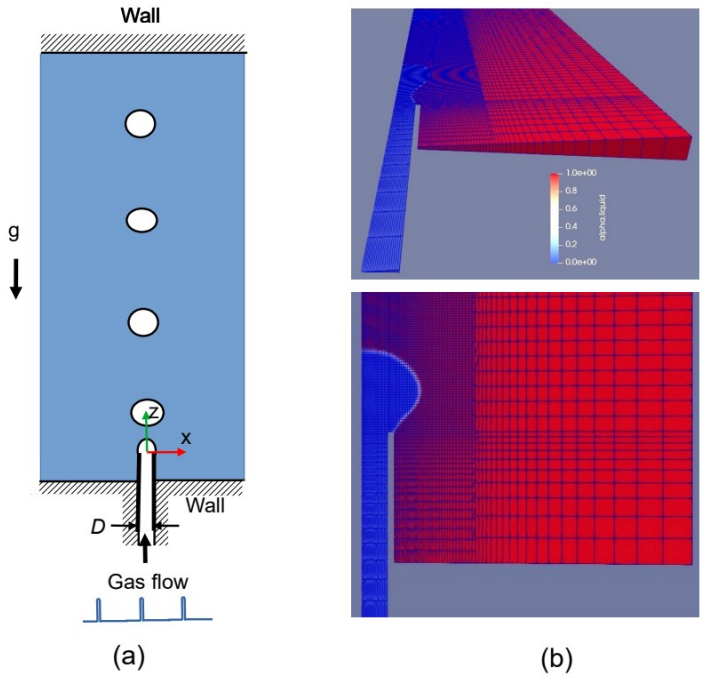

Fig. 1 (a) Schematic of bubble formation when a gas flows through an upward-pointing needle into a liquid tank; (b) A wedge mesh (discretized into quadrilateral finite-volume cells in two-dimensional space) with a combination of fine and coarse patches, used for simulations of the axisymmetric two-phase flows in the present bubble formation problem. The top boundary of the computational domain is located at 33 × *D* from the needle tip, such that its effect on bubble formation becomes inconsequential and is treated as a wall for computational simplicity.

As done in a recent work by Feng [3], the chosen solver for this type of two-phase flow problem is named interIsoFoam—an improved geometric VOF solver detailed by Roenby et al. [11], Gamet et al. [12], and reviewed by Mulbah et al. [13] as a

scheme for high accuracy at low computational cost. Because the description of this type of VOF solver is available in published literature [12 - 14], it is unnecessary to repeat the details here. Briefly in simple terms, the VOF method treats the fluid interface as the "jump" of a scalar phase fraction field from 0 to 1, located in those cells containing fraction values (other than 0 and 1) in an Eulerian mesh. Movements of the scalar phase fraction are governed by a transport equation describing the advection of it with the flow. Then, the traction boundary condition at the free interface is transformed into a body force term associated with the gradient of the scalar phase fraction field in the Navier-Stokes momentum equations in an Eulerian frame, eliminating the need to deal with a moving mesh. It especially makes the simulations of bubble-detaching dynamics much less challenging.

In the present work for most cases, the nominal values for liquid phase density and dynamic viscosity are ρ = 1000 kg m^{-3} and μ = 0.001 kg m^{-1} s^{-1} (i.e., 1 cp, unless otherwise specified), whereas those corresponding to the gas phase are ρ_g = 1.2 kg m^{-3} and μ_g = 1.8X10^{-5} kg m^{-1} s^{-1} (0.018 cp), respectively specified for the VOF computations. Over orders-of-magnitude contrasts between liquid and gas phases in terms of these corresponding values would make the influence of gas-phase density and viscosity on the general fluid dynamical behavior almost irrelevant; therefore, only the liquid density and viscosity are considered in the analysis and discussion. The nominal surface tension value at the gas-liquid interface is taken as σ = 0.07 kg s^{-2} (unless otherwise specified), closely representing the air-water situation.

To complete the case specification, the boundary conditions used at the gas inlet are zeroGradient for the piezometric pressure p (cf. Description in Feng [15]) and the uniform fixed value type for the velocity vector $U = (0, 0, U_z)$ with

$$U_z(t) = \begin{cases} U_a \text{ for } n\Delta T < t < n\Delta T + \Delta\tau \text{ with } n = 0, 1, 2... \\ 0 \quad \text{for any other time } t \end{cases}, \tag{1}$$

where U_a = constant denoting the rectangular-wave pulse amplitude of gas inlet velocity, $\Delta\tau$ the pulse width, and ΔT the pulse cycle period. At solid walls, the noSlip type for U and zeroGradient for p are applied. At the open lateral boundary, the pressureInletOutletVelocity condition for U and a fixed value type for p (e.g., = 10^5 Pa) are applied.

At the gas-liquid-solid three-phase contact line, the available dynamicAlphaContactAngle condition is applied as is by specifying the static contact angle θ_0, advancing contact angle θ_A, and receding contact angle θ_R, as well as a u_q value. Here, for a specified static contact angle θ_0 the advancing contact angle and receding contact angle are always assigned as $\theta_A = \theta_0 + 15^\circ$ and $\theta_R = \theta_0 - 15^\circ$ with a fixed value of u_q (i.e., = 1 m s^{-1}) to keep the presentation logically streamlined and self-consistent. Without losing generality, computed cases in the present work would have a nominal contact angle $\theta_0 = 45^\circ$ (corresponding to a partially wetting liquid at the solid wall) unless otherwise specified.

As mentioned in Feng [3], each OpenFOAM® solver comes with at least one tutorial case. In fact, many popular solvers could have multiple tutorial cases provided with the standard downloadable packages. This can be very convenient for users who would not want to spend much time deciphering the exact meanings of those numerical scheme parameters; some of the tutorial parameter settings can indeed be directly used for similar computational problems. The numerical scheme parameters used in the present work for fvScheme and fvSolution are directly copied from the interIsoFoam tutorial case of "damBreak", using the typical "Euler" implicit time scheme for temporal integration with an adjustable time step under the restriction of Courant number < 0.2.

3. Results and Discussion

With pulsating gas flows (at θ_0 = 45°), Fig. 2 shows that air bubbles of d = 1.738, 0.909, 0.196, 0.114 mm in water from needles of D = 1, 0.5, 0.1, 0.05 mm can be obtained, with U_a = 5, 5, 10, 20 m/s and $\Delta\tau$ = 0.7, 0.4, 0.05, 0.02 ms, corresponding to V = 0.25 π D^2 U_a $\Delta\tau$ = 2.749, 0.393, 0.00393, 0.000785 mm^3 . It should be noted that here in this work, the presented values of pulse width $\Delta\tau$ are about their minima for reliable one-per-pulse bubble detachment. Hence, the corresponding values of d represent the smallest bubble diameters practically feasible under given conditions. It appears possible to obtain d < 2 D with pulsating gas flows even for needle orifices of D << 1 mm. An inspection of the computed results for the transient bubble formation process indicates the fact that the time from pulse initiation for bubble detachment τ is much longer than the pulse width $\Delta\tau$ (as quantitatively presented in Table 1).

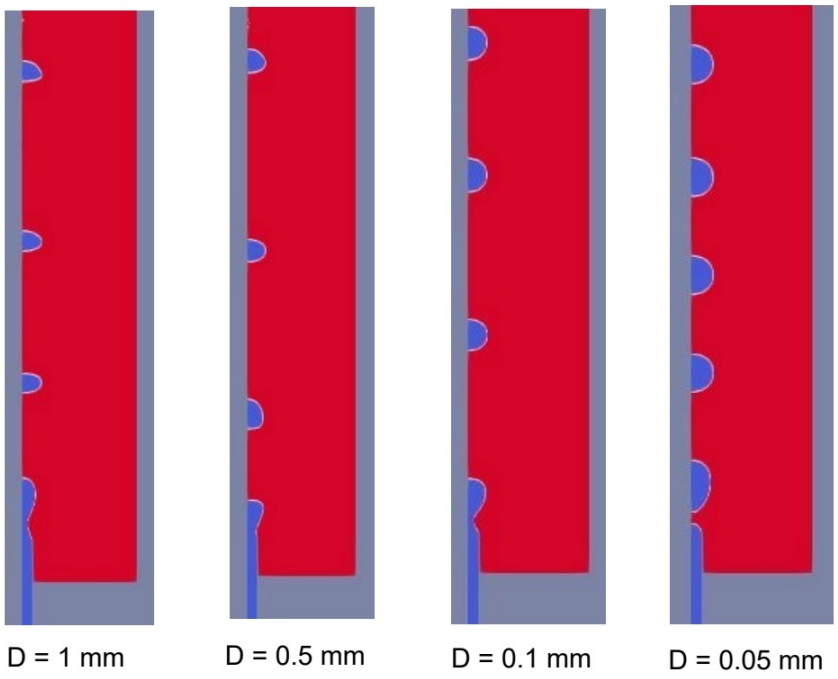

Fig. 2 Air bubbles of d = 1.738, 0.869, 0.196, 0.114 mm generated in water from needles of D = 1, 0.5, 0.1, 0.05 mm (at U_a = 5, 5, 10, 20 m/s respectively with $\Delta\tau$ = 0.7, 0.4, 0.05, 0.02 ms and ΔT = 20, 10, 2, 0.5 ms), simulated with the OpenFOAM® VOF solver interIsoFoam and visualized with the postprocessor ParaView

Table 1. Computational results of detachment time τ of air bubbles generated from various needle orifice diameters *D* corresponding to given pulse parameter values U_a and $\Delta\tau$ in (1), which determine the detached bubble volume *V* and diameter *d*

D (mm)	U_a (m/s)	$\Delta\tau$ (ms)	*V* (mm^3)	*d* (mm)	τ (ms)
1	5	0.7	2.749	1.738	7.52
0.5	5	0.4	0.393	0.909	3.31
0.1	10	0.05	0.00393	0.196	0.407
0.05	20	0.02	0.000785	0.114	0.138

Intuitively in terms of physics, once an adequate of amount of gas is pushed out of the needle orifice, the time for neck pinch-off of gas-liquid interface to complete, (τ - $\Delta\tau$) / t_σ, is likely to relate to the capillary timescale [2],

$$t_\sigma = \sqrt{\frac{\rho D^3}{8\sigma}} \ , \qquad (2)$$

which becomes 1.336, 0.472, 0.0423, 0.0149 ms for *D* = 1, 0.5, 0.1, 0.05 mm (with ρ = 1000 kg m^3 and σ = 0.07 kg s^{-2}). Hence, the corresponding values of (τ - $\Delta\tau$) / t_σ are 6.151, 7.853, 10.815, 10.575 respectively for *D* = 1, 0.5, 0.1, 0.05 mm in Table 1. To avoid coalescence among a train of periodically released bubbles, the pulse cycle period $\Delta T > 2\ \tau$ (or > 20 x t_σ) might be desired.

The transient bubble free-surface profiles are shown in Fig. 3 during the bubble detachment process at *t* ~ 0, $\Delta\tau$, τ, and so forth, corresponding to the cases in Fig. 2 and Table 1. Around *t* = 0 when pulsating gas flow starts, the meniscus profile takes a

nearly circular shape with the contact line pinned at the needle inner orifice edge. After the pulsating gas flow stops at $t = \Delta\tau$, the free surface tends to take an oblate spheroidal profile with the contact line located at the needle outer edge. Then, the contact line would move back to the orifice edge during the free surface neck formation and pinch-off process, and thereafter.

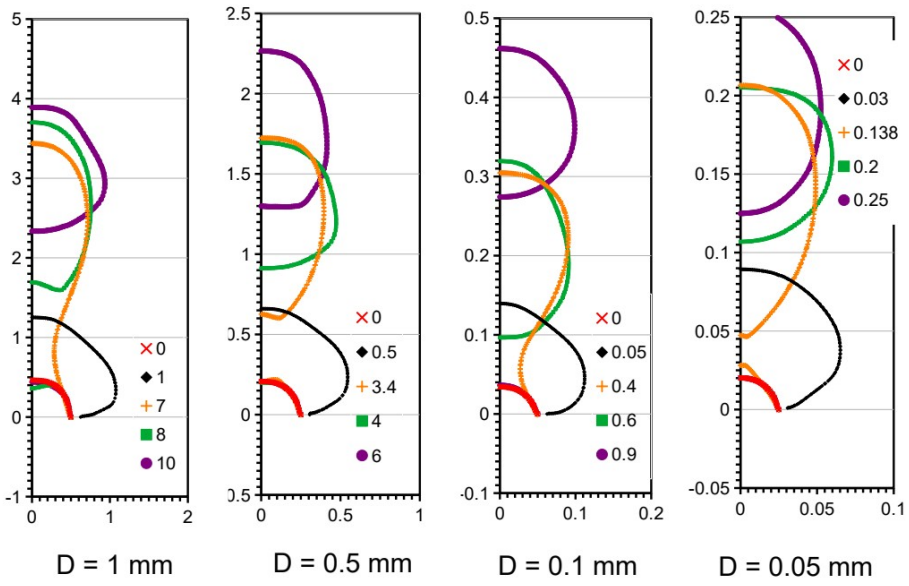

Fig. 3 Free surface shapes during air bubble formation from needles of D = 1, 0.5, 0.1, 0.05 mm (at U_a = 5, 5, 10, 20 m/s respectively with $\Delta\tau$ = 0.7, 0.4, 0.05, 0.02 ms). The axis labels here are in units of millimeter (mm) and curve legend labels in units of millisecond (ms) with respect to the time of pulse initiation.

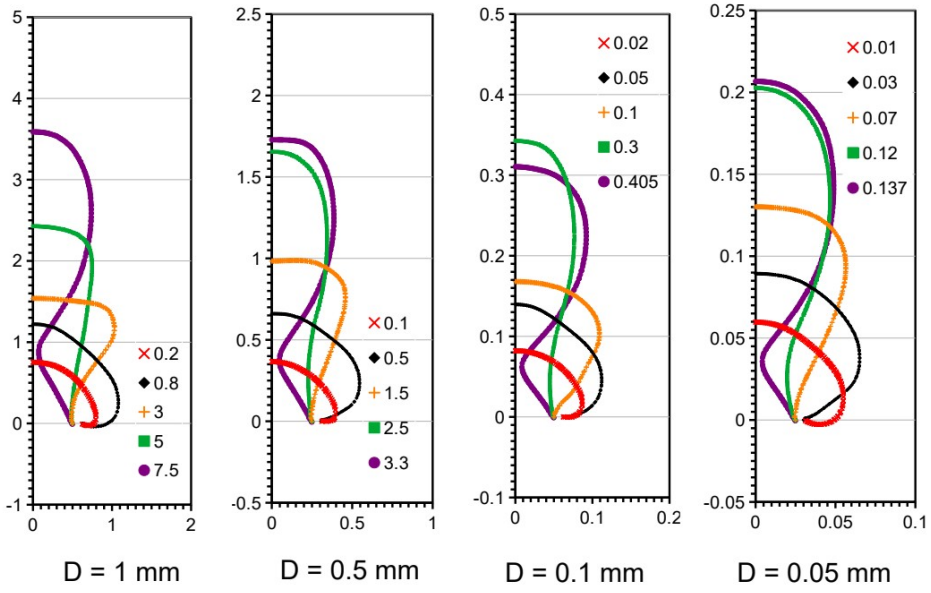

Fig. 4 As Fig. 3 but for free surface evolution up to necking pinch-off.

More details of free surface shape evolution of the attached bubbles before their pinch-off are shown in Fig. 4, for the corresponding cases in Fig. 2. Clearly, during the pulsating flow time ($0 < t < \Delta\tau$), the oblate meniscus grows nonuniformly with more significant lateral expansion while the contact line can be pushed over the needle outer edge (more so with increasing U_a). Such a deviation from the static meniscus shape of a circular profile with uniform curvatures is the consequence of nonuniform stress

distribution associated with substantial fluid flow around. Once the pulsating flow disappears (after $t = \Delta\tau$), the deformed meniscus would attempt to recover the static equilibrium shape driven by the capillary force. This meniscus rebounding would perpetuate an upward stretching of the meniscus front, causing contact line retraction to the needle inner orifice and thereby a neck formation, until the bubble pinch-off.

It might be noticed that the cases in Table 1 corresponding to Fig. 2 suggest a tendency of increasing U_a, to enable generating smaller bubbles with reducing needle size while maintaining $d \sim 2 \times D$ or less. Why so deserves further investigation.

3.1 Effect of pulse amplitude

For D = 1 mm, if the pulse amplitude of gas inlet velocity U_a is reduced from 5 m/s (as in Table 1) to 1 m/s, air bubbles in water may only be generated with $\Delta\tau$ = 10 ms (for V = 7.85 mm^3 and d = 2.47 mm, cf. Table 2), but cannot with $\Delta\tau$ = 5 ms for smaller bubble size of V = 3.93 mm^3 and d = 1.96 mm. On the other hand, increasing U_a to 10 m/s makes the generation of even smaller bubbles possible with $\Delta\tau$ = 0.25 ms (for V = 1.96 mm^3 and d = 1.55 mm). The higher pulse amplitude at U_a = 10 m/s tends to result in much more significant deformations of the meniscus than those of U_a = 1 and 5 m/s during bubble growth and detachment (as illustrated in Fig. 5). A more significantly deformed meniscus leads to a stronger meniscus rebound for quicker pinch-off bubble detachment. It becomes obvious now that increasing the pulse amplitude enables the

generation of smaller bubbles with substantially shorter pulse widths for a given needle size.

Table 2. As Table 1 but for D = 1 mm with various U_a , etc.

D (mm)	U_a (m/s)	$\Delta\tau$ (ms)	V (mm^3)	d (mm)	τ (ms)
	1	10	7.854	2.466	22.5
1	5	0.7	2.749	1.738	7.52
	10	0.25	1.963	1.554	1.91

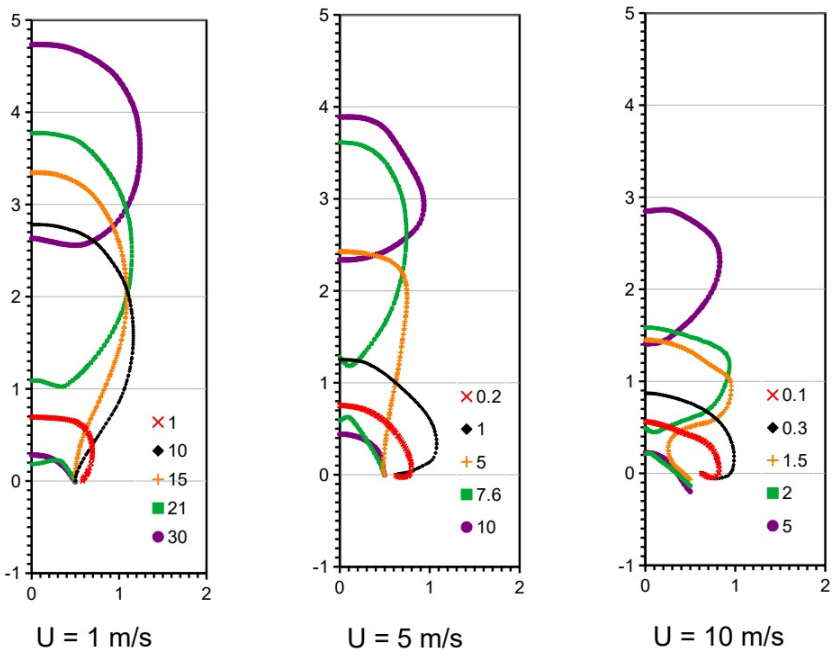

Fig. 5 As Fig. 3 but for D = 1 mm at U_a = 1, 5, 10 m/s with $\Delta\tau$ = 10, 0.7, 0.25 ms (ΔT = 50, 20, 20 ms)

The value of U_a can be closely related to the impulse or momentum input of pulsating gas flow, $\rho_g \pi D^2 U_a^2 \Delta\tau / 4$. The force associated with such an impulse may be expressed as:

$$F = \frac{\rho_g \pi D^2 U_a^{\,2}}{4} \quad . \tag{3}$$

If measured in units of the buoyancy force ($\rho V g$) or capillary force ($\sigma \pi D$), the impulse force F_b or F_σ (which directly relates to the familiar Weber number *We*) would take the forms:

$$F_b = \frac{\rho_g U_a}{\rho g \Delta\tau} \text{ or } \quad F_\sigma = \frac{\rho_g U_a^{\,2} D}{4\sigma} = \frac{\rho_g}{4\rho} \times \left(\frac{\rho U_a^{\,2} D}{\sigma} \right) = \frac{\rho_g}{4\rho} \times We \ , \tag{4}$$

both of which indicate an increasing impulse effect with U_a on the bubble formation process. For the air bubble in water cases in Table 2 and Fig. 5, the increasing values of F_b and F_σ are shown in Table 3 along with the corresponding decreasing values of (τ - $\Delta\tau$) / t_σ and d / D as U_a increases with shrinking $\Delta\tau$.

Table 3. As Table 2 but for values of F_b , F_σ , $(\tau - \Delta\tau) / t_\sigma$, and d / D

D (mm)	U_a (m/s)	$\Delta\tau$ (ms)	F_b	F_σ	$(\tau - \Delta\tau) / t_\sigma$	d / D
	1	10	0.0122	0.0043	9.354	2.466
1	5	0.7	0.874	0.1071	6.151	1.738
	10	0.25	4.893	0.4286	1.616	1.554

Reducing the needle orifice to D = 0.5 mm shows a similar general trend, as shown in Table 4. For the cases in Table 4 and Fig. 6, the values of F_b and F_σ shown in Table 5, along with the corresponding values of $(\tau - \Delta\tau) / t_\sigma$ and d / D exhibit similar general trends as in Table 3.

Table 4. As Table 2 but for D = 0.5 mm

D (mm)	U_a (m/s)	$\Delta\tau$ (ms)	V (mm^3)	d (mm)	τ (ms)
	1	20	3.927	1.957	26.3
0.5	5	0.4	0.393	0.909	3.31
	10	0.18	0.353	0.877	3.81

However, the value of $(\tau - \Delta\tau) / t_\sigma$ for U_a = 10 m/s is slightly greater than that for U_a = 5 m/s, apparently as a consequence of contact line sliding down on the outside needle wall for U_a = 10 m/s in Fig. 6 when the pulsating flow is activated. Such an outward contact line motion at U_a = 10 m/s in Fig. 6 does not seem to occur for the

corresponding case for D = 1 mm in Fig. 5 (consistent with the findings of a constant gas flow study [3], i.e., increasing U_a and reducing D both promote outward contact line motion from the orifice.)

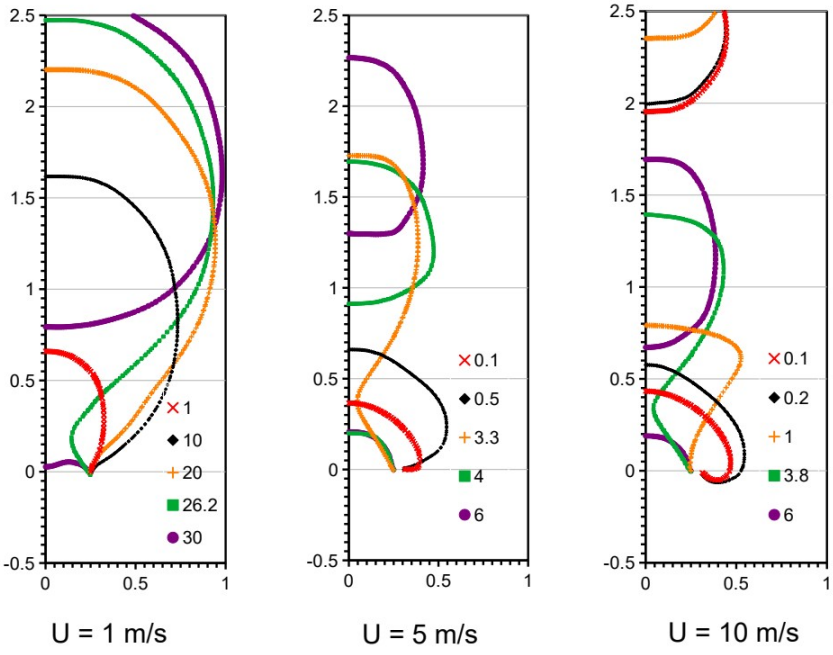

Fig. 6 As Fig. 3 but for D = 0.5 mm at U_a = 1, 5, 10 m/s with $\Delta\tau$ = 20, 0.4, 0.18 ms (ΔT = 50, 10, 10 ms)

As revealed with a series of comparative cases [3], increasing U_a tends to unpin the contact line at the needle inner edge and cause contact line sliding on the orifice outside wall that leads to increased bubble size. This phenomenon is consistently illustrated in Figs. 5 and 6 for the cases of U_a = 1, 5, 10 m/s (with θ_0 = 45°). However,

the effect of such contact line movement on bubble size is considerably restricted with the usage of thin-wall needles, as expected when compared with simply an orifice on a flat surface. With relatively low U_a (e.g., 1 m/s, $F_b << 1$, $F_\sigma < 0.01$ or $We < 33$), the contact line appears to be pinned at the needle inner edge, except for a short moment around $t \sim 1$ ms with the case of $D = 1$ mm when the contact line exhibits a slight movement on the horizontal wall of the needle orifice.

Table 5. As Table 3 but for $D = 0.5$ mm

D (mm)	U_a (m/s)	$\Delta\tau$ (ms)	F_b	F_σ	$(\tau - \Delta\tau) / t_\sigma$	d / D
	1	20	0.00612	0.0021	97.999	3.914
0.5	5	0.4	1.529	0.0536	7.853	1.818
	10	0.18	6.796	0.2143	8.445	1.754

However, with $U_a = 1$ m/s ($F_b << 1$, $F_\sigma < 0.01$ or $We < 33$), the advantage of pulsating gas flow for producing small bubbles would not be significant, e.g., the values of d / D in Tables 3 and 5 approach those estimated for low constant gas flow (2.60 and 4.12 mm for $D = 1$ and 0.5 mm). As U_a increases to 5 and 10 m/s ($F_b > 1$, $F_\sigma >> 0.01$), the contact line would move over the outer needle edge when the pulsating gas flow is activated, and then would come back to the inner needle edge during the necking pinch-off process. At $U_a = 10$ mm/s, the contact line could be pushed down along the needle inner wall of the $D = 1$ mm orifice around the time of free surface pinch-off, but not so noticeable with the $D = 0.5$ mm orifice. With a large pulse amplitude $U_a = 10$ mm/s

during activated gas flow, the contact line tends to be unpinned from the outer needle edge and slide downward on the needle outer wall, which seems to hinder the meniscus rebounding process after the pulsating gas flow is shut off and thereby makes generating smaller bubbles more difficult.

For smaller orifices such as D = 0.1 (or 0.05) mm, even at U_a ~ 5 (or 10) m/s, the value of F_σ would become ~0.011 (or 0.021), not capable of generating bubbles of d / D < 6, rendering diminished effectiveness of pulsating gas flow for reducing bubble size. Data in Tables 3, 5, 6 indicate that bubbles of d / D < 2 can be generated with F_σ > 0.04 (corresponding to We > 133) with D > 0.1 mm, but with D = 0.05 mm it appears difficult to obtain d / D < 2; even at U_a = 40 m/s (We ~ 1143) the value of d / D would still be greater than 2.12.

Table 6. As Table 3 but for D = 0.1 and 0.05 mm

D (mm)	U_a (m/s)	$\Delta\tau$ (ms)	F_b	F_σ	$(\tau - \Delta\tau) / t_\sigma$	d / D
0.1	9	0.09	12.232	0.0347	7.454	2.299
	20	0.021	116.50	0.1714	8.921	1.847
0.05	15	0.03	61.162	0.0482	12.048	2.381
	40	0.008	611.62	0.3429	9.036	2.125

All the cases computed here thus far have been with the contact angle θ_0 = 45° for air bubbles in water, which represents the case favorable to small bubble detachment with liquid adequately wetting the orifice wall [3]. What would happen if

this contact angle deviates from 45° on the needle wall with pulsating gas flow through thin-wall needles?

3.2 Effect of contact angle

Increasing the contact angle, θ_0 , corresponds to less wetting liquids on the needle wall, which is expected to enhance outward motion of the contact line on the needle wall from the orifice [3]. As shown in Table 7 and Fig. 7 for D = 0.5 mm at U_a = 10 m/s (F_σ = 0.2143 or We ~ 714), with increasing θ_0 the detached bubble size indeed increase along with enhance outward contact line motion on the needle walls, i.e., d / D = 1.75, 1.96, 2.47 for θ_0 = 45° (as well as 30°), 75°, 90° .

Table 7. As Table 2 but for D = 0.5 mm at U_a = 10 m/s

D (mm)	θ_0 (deg)	$\Delta\tau$ (ms)	V (mm^3)	d (mm)	τ (ms)
0.5	30	0.18	0.353	0.877	3.32
	45	0.18	0.353	0.877	3.81
	75	0.25	0.491	0.979	3.84
	90	0.50	0.982	1.233	5.73

The same trend is also reflected for the case of D = 0.1 mm, i.e., with U_a = 10 m/s at θ_0 = 45° and 75° , we obtain d / D = 1.96 and 2.29 with $\Delta\tau$ = 0.05 and 0.08 ms, respectively. If U_a is increased to 20 m/s, then d / D become 1.85 and 2.06 with $\Delta\tau$ = 0.021 and 0.029 ms, respectively at θ_0 = 45° and 75° (for D = 0.1 mm).

The case of air bubbles in water investigated so far, with μ = 1 cp and σ = 0.07 kg s^{-2} , represents the situation of relatively low liquid viscosity and high surface tension among liquids commonly encountered in realistic applications. For many liquids, the value of viscosity can vary by orders of magnitude. Thus, it is important to examine the effect of liquid viscosity in bubble formation with pulsating gas flow.

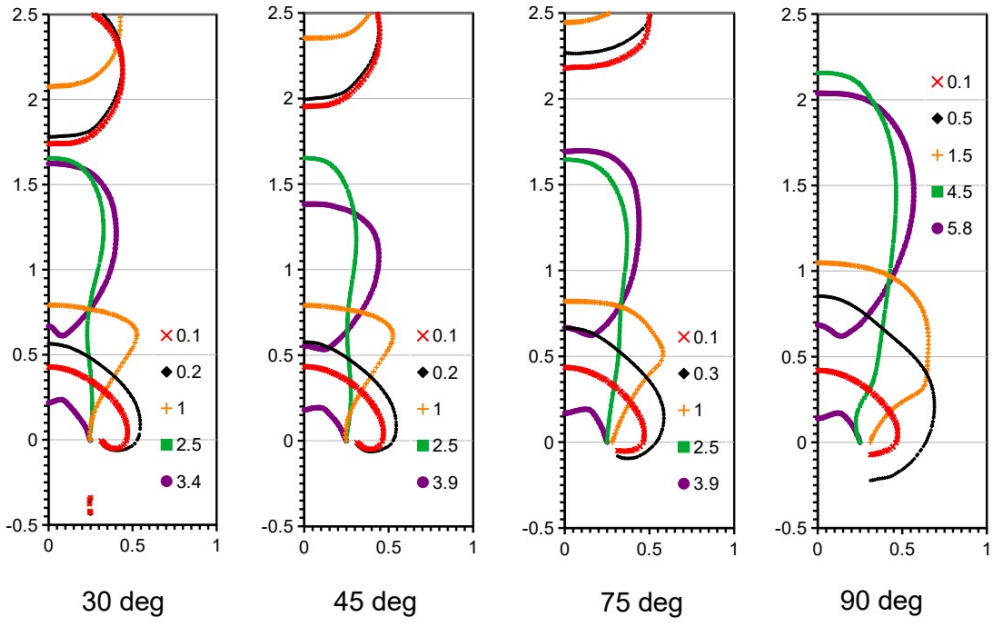

Fig. 7 As Fig. 3 but for D = 0.5 mm at U_a = 10 m/s with $\Delta\tau$ = 0.18, 0.18, 0.25, 0.5 ms for θ_0 = 30°, 45°, 75°, 90° (ΔT = 10, 10, 10, 20 ms)

3.3 Effect of liquid viscosity

Now, as it becomes clear that the resulting liquid flow driven by the input momentum of pulsating gas flow plays a crucial role in effectively reducing detached bubble size, the damping effect of liquid viscosity to the liquid flow intensity could be significant here. To quantitatively illustrate the liquid viscosity effect, a set of cases with various values of μ are computed and shown in Table 7 for needles of D = 0.1 mm (for θ_0 = 45°).

Table 7. As Table 1 but for μ = 1, 2 and 4 cp with D = 0.1 mm at various values of U_a

μ (cp)	U_a (m/s)	$\Delta\tau$ (ms)	V (mm^3)	d (mm)	τ (ms)
1	10	0.05	0.00393	0.196	0.407
	20	0.021	0.0033	0.185	0.356
2	10	0.25	0.0196	0.335	0.841
	20	0.039	0.00613	0.227	0.453
4	20	0.17	0.0267	0.371	0.895
	40	0.055	0.0173	0.321	0.878

For low viscosity liquids such as water with μ ~ 1 cp (or 0.001 kg m^{-1} s^{-1}), bubbles of d / D < 2 can be robustly generated with D = 0.1 mm at U_a = 10, 20 m/s (F_σ = 0.043, 0.171 or We ~ 143, 573). As the liquid viscosity μ is increased to 2 cp, it becomes impossible to generate bubbles of d / D < 2 with the same needles and U_a values; the pulse width $\Delta\tau$ must be increased for larger bubbles with enhanced buoyant force to compensate for the viscous loss of liquid flow intensity for reliable pinch-off

detachment. With liquids of μ ~ 4 cp, bubbles of d / D < 4 could hardly detach at U_a < 20 m/s (for a needle of D ~ 0.1 mm). Hence, the minimum feasible bubble size generated with pulsating gas flow appears to be very sensitive to the liquid viscosity, unlike the situation with constant gas flow where the detached bubble size is shown insensitive to the liquid viscosity (experimentally by Helsby and Tuson [16] as well as numerically by Ohta et al. [11] and Feng [3], especially under the quasi-static condition).

To evaluate the liquid flow inertial effect versus viscous effect, it is common in fluid dynamics to consider the value of the Reynolds number,

$$Re = \frac{\rho U_a D}{\mu} \quad , \tag{5}$$

which becomes 1000 for ρ = 1000 kg m^{-3} , μ = 0.001 kg m^{-1} s^{-1} (= 1 cp), U_a = 10 m/s, D = 0.1 mm (= 10^{-4} m). Then, we would have Re = 500, 250 for μ = 2, 4 cp, if all other parameters remain the same. If the viscosity is reduced to μ = 0.5 cp, the value of Re would become 2000 with U_a = 10 m/s, the same as that with μ = 1 cp and U_a = 20 m/s. However, with U_a = 10 m/s and μ = 0.5 cp, bubbles of d / D ~ 1.82 can be obtained with $\Delta\tau$ ~ 0.04 ms, practically comparable to d / D ~ 1.85 with U_a = 20 m/s and μ = 1 cp (shown in Table 6), at the same value of Re = 2000.

For D = 0.5 mm at Re = 1000 or 2000, the corresponding value of U_a should be 2 or 4 m/s with μ = 1 cp, which would enable producing bubbles of d ~ 1.89 mm (d / D ~ 3.6) with $\Delta\tau$ ~ 7.8 ms or d ~ 0.896 mm (d / D ~ 1.79) with $\Delta\tau$ ~ 0.48 ms. Similarly, for D

= 1 mm, bubbles of d / D ~ 1.98 can be generated with $\Delta\tau$ ~ 2.6 ms at *Re* = 2000 (with U_a = 2 m/s and μ = 1 cp), while d / D > 2.47 at *Re* = 1000 (with U_a = 1 m/s and μ = 1 cp, shown in Table 3). Thus, the present results seem to suggest that *Re* > 2000 is required to robustly obtain bubbles of d / D ~ 2 or smaller (for D < 1 mm and σ = 0.07 kg s^{-2}), while *Re* = 1000 could enable d / D < 4 in general and d / D ~ 2 in some circumstances.

Table 8. Values of *Re* , *Ca* and *Oh* corresponding to cases in Table 7 (for σ = 0.07 kg s^{-2})

μ (cp)	U_a (m/s)	*Re*	*Ca*	*Oh*	d / D
1	10	1000	0.1429	0.002313	1.96
	20	2000	0.2857		1.85
2	10	500	0.2857	0.004625	3.35
	20	1000	0.5714		2.27
4	20	500	1.1429	0.00925	3.71
	40	1000	2.2857		3.21

Besides the value of *Re* in (5), the values of capillary number (*Ca*) and Ohnesorge number (*Oh*),

$$Ca = \frac{\mu U_a}{\sigma} \quad \text{and} \quad Oh = \frac{\mu g^{1/4}}{\rho^{1/4}\sigma^{3/4}} \ , \tag{6}$$

can also substantially influence the bubble formation process and detached bubble size, even the value of *Re* remains the same, as shown in Table 8 and Fig. 8. It should be note

that here *Ca* = *We* / *Re* can be calculated from known values of Weber and Reynolds numbers.

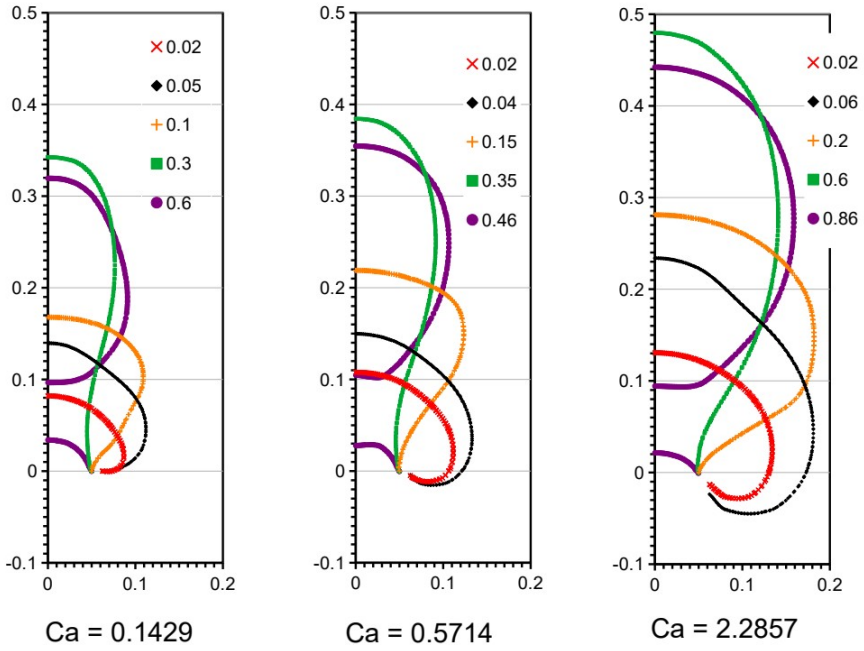

Fig. 8 As Fig. 3 but for D = 0.1 mm at Re = 1000 with μ = 1, 2, 4 cp corresponding to U_a = 10, 20, 40 m/s respectively with $\Delta\tau$ = 0.05, 0.039, 0.055 ms (as in Table 8)

A trend for the feasible bubble size generated with pulsating gas flows to increase with the values of *Ca* and *Oh* appears clear, for a given value of *Re* . When the value of *Ca* becomes large (e.g., *Ca* = 2.2857), the relative strength of surface tension force (with respect to viscous force) might be insufficient to hold the contact line from sliding over the needle outside wall, yielding larger detached bubbles [3, 10].

3.4 Effect of surface tension

An analysis of static force balance between surface tension and buoyancy [17-19] indicates that the detached bubble volume tends to be proportional to surface tension σ, corresponding to bubble diameter proportional to $\sigma^{1/3}$, for very low gas flow rates in the constant gas flow situation. But for substantially reducing the bubble size with pulsating gas flows, whether reducing surface tension σ can still help reduce the bubble size deserves a sincere investigation.

Table 9. As Table 7 but for σ = 0.035 kg s^{-2} (representative to the situation of air bubbles in various non-aqueous liquids)

μ (cp)	U_a (m/s)	$\Delta\tau$ (ms)	V (mm^3)	d (mm)	τ (ms)
1	10	0.05	0.00393	0.196	0.534
	20	0.026	0.00408	0.198	0.533
2	10	0.155	0.0122	0.285	0.933
	20	0.061	0.00958	0.264	0.919
4	20	0.173	0.0272	0.373	1.568
	40	0.081	0.0254	0.365	1.632

Table 9 shows a set of computed results with σ = 0.035 kg s^{-2} for μ = 1, 2, 4 cp (with θ_0 = 45° and ρ = 1000 kg m^{-3}), to directly compare with the σ = 0.07 kg s^{-2} cases in Table 7. Now the values of *Oh* would become 1.6818 times those in Table 7. For pulsating gas flow to effectively reduce bubble size (e.g., with *Re* > 1000), reducing

surface tension may not be helpful. Instead of generating smaller bubbles, lower surface tension liquids could yield larger bubbles generated with comparable pulse amplitudes of pulsating gas flow, in sharp contrast to those with constant gas flow (for quasi-static situations).

Table 10. Values of σ, *Ca* and *Oh* at *Re* = 2000 with a *D* = 0.5 mm needle

μ (cp)	U_a (m/s)	σ (kg s^{-2})	*Ca*	*Oh*	*d* / *D*
1	4	0.07	0.05714	0.002313	1.79
		0.035	0.1143	0.003889	1.6
2	8	0.07	0.2286	0.004625	1.71
		0.035	0.4571	0.007779	1.79
4	16	0.07	0.9143	0.00925	1.93
		0.035	1.8286	0.01556	1.79

With a needle of *D* = 0.5 mm (θ_0 = 45°) at *Re* = 2000, Table 10 shows the normalized bubble size *d* / *D* for various values of surface tension σ and liquid viscosity μ, where the tabulated data seem lacking a clear regularity in terms of the effects of varying *Ca* and *Oh* on minimum feasible bubble sizes. When a broader range of computed data of *d* / *D* versus *We* is plotted in Fig. 9, the primary trends become clear by ignoring some of the fine-granularity noise due to different *Oh* values. For generating bubbles of *d* / *D* < 2, there exists a lower limit of the *We* value below which the (minimum feasible) value of *d* / *D* would increase abruptly, for a given needle diameter

D and a value of *Re* . For example, at *Re* = 2000, it seems possible to generate bubbles of *d* / *D* < 2 with needles of *D* ~ 0.5 mm as long as *We* > 60, but needles of *D* ~ 0.1 mm would require *We* > 100. It *Re* is reduced to 1000, it would need 60 < *We* < 600 with needles of *D* ~ 0.5 mm for generating bubbles of *d* / *D* < 2, while the range shrinks to 100 < *We* < 300 for needles of *D* ~ 0.1 mm.

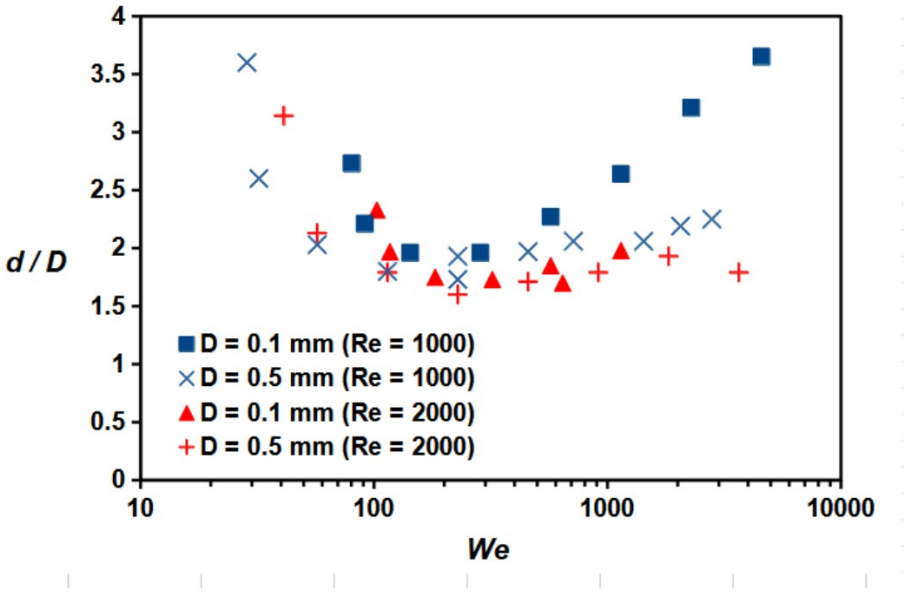

Fig. 9 Computed data of *d* / *D* versus *We* for *D* = 0.1 and 0.5 mm at *Re* = 1000 and 2000

When the value of *We* is reduced below the lower limit for *d* / *D* < 2 (e.g., *We* ~ 60 for *D* ~ 0.5 mm and *We* ~ 100 for *D* ~ 0.1 mm), the bubble size would become very

sensitive to a slight change of *We* ; the value of *d* / *D* increases rapidly with even a small amount of further reduction of *We* as seen in Fig. 9. Moreover, the value of *d* / *D* appears to become more sensitive to *We* with reduction of the needle size, i.e., the range of *We* for *d* / *D* < 2 decreases when using smaller needles. On the other hand, increasing the value of *Re* can reduce the sensitivity of *d* / *D* to *We* (as shown in Fig. 9 with the contrast between cases of *Re* = 1000 and 2000).

For smaller needles of *D* = 0.05 mm, however, Table 6 shows the difficulty to obtain *d* / *D* < 2 (e.g., *d* / *D* > 2.12 even with U_a = 40 m/s for μ = 1 cp and σ = 0.07 kg s^{-2}, *Re* = 2000 and *We* = 1143, in an air-water system). But a reduction of μ to 0.5 cp at U_a = 40 m/s (*Re* = 4000 and *We* = 1143 for *D* = 0.05 mm) seems to be able to bring the value of *d* / *D* down to 1.82 (with $\Delta\tau$ = 0.005 ms), and an additional reduction of σ to 0.035 kg s^{-2} (*Re* = 4000 and *We* = 2286) could get *d* / *D* further down to 1.75 (with $\Delta\tau$ = 0.0045 ms). Thus, using smaller needles for generating bubbles of *d* / *D* < 2 may require increasing *Re* and *We* for practical effectiveness. This makes the usage of smaller needles more challenging for reducing bubble size in liquids of relatively high viscosity.

In contrast, larger needles can be much easier in generating bubbles of reduced sizes in liquids of relatively higher viscosity with moderate pulse amplitudes. For example, it seems quite difficult to obtain bubbles of *d* / *D* < 2 with needles of *D* = 0.1 mm in liquids of μ > 4 cp even with U_a = 40 m/s (cf. Tables 7-9, for *Re* = 1000, *We* ~ 2286 and 4571). If a needle of *D* = 1 mm is used, bubbles of *d* / *D* ~ 1.85 or 1.72 (for σ = 0.07 or 0.035 kg s^{-2} , *Re* = 1000, *We* ~ 1429 or 2857) can be generated with U_a = 10 m/s in liquids of μ = 10 cp.

3.5 Bubble throughput

According to a recent study of Feng [3], the computed air bubble volumes generated in a water tank with constant gas flow (at diminishing flowrate) through orifices of various diameters *D* compare well with the fitted power law of Bari and Robinson [20] for experimentally measured quasi-static bubble volume V_B in experiments with fixed contact lines:

$$\frac{V_B}{V_F} = 0.6863 \left(\frac{D}{L_\sigma} \right)^{-0.116} \quad \text{with } V_F = \frac{\sigma \pi D}{\rho g} \quad \text{and} \quad L_\sigma = \sqrt{\frac{\sigma}{\rho g}} \quad , \tag{7}$$

with the corresponding bubble diameters in water for *D* = 1, 0.5, 0.1, and 0.05 mm becoming $d_B = (6 V_B / \pi)^{1/3}$ = 3.21, 2.61, 1.63, and 1.33 mm, respectively, as references here for comparison.

For reducing the detached bubble size, using a pulsating gas flow is practically desired to offer reasonable gas throughput in comparison with that of a constant gas flow. As often demonstrated in the present work, the bubble detachment time τ (from pulse initiation) is typically about ten times the capillary timescale t_σ in (2). Therefore, to avoid interaction and coalescence among detached bubbles, it is usually safe to use the pulse cycle period $\Delta T > 2\ \tau$ (or > 20 × t_σ). Here in Table 11, the value of ΔT is assumed to be 2.5 τ for a conservative estimate of gas bubble throughput $Q = \pi d^3 / (6\ \Delta T)$.

Table 11 provides the computed data for evaluating the gas throughput values of smallest air bubbles generated in water at Re = 2000 from needles of various sizes with pulsating gas flows, compared with the representative quasi-static bubble sizes for constant gas flow cases at $Q / Q_{crit} << 1$ according to

$$d_B = \left(\frac{6 V_B}{\pi} \right)^{1/3}, \quad Q_{crit} = \pi \left(\frac{16}{3 g^2} \right)^{1/6} \left(\frac{\sigma D}{2 \rho} \right)^{5/6} \quad . \tag{8}$$

Here, the value of V_B is calculated from the formula in (7) based on the experimental values for $Q / Q_{crit} << 0.1$, where Q_{crit} is regarded as the critical constant gas flowrate below which the bubble formation process may be theoretically assumed as quasi-static with detached bubble size being insensitive to significant change in gas throughput [2].

Table 11. Computed minimum feasible bubble diameters d and detachment time τ in water at Re = 2000 for various needle orifice diameters D with derived pulsating gas flow throughput Q , to compare with d_B and Q_{crit} in (8)

D (mm)	t_σ (ms)	d (mm)	τ (ms)	Q (μL/s)	d / d_B	Q / Q_{crit}
1	1.336	1.98	8.88	183.08	0.617	0.155
0.5	0.472	0.895	4.69	32.02	0.341	0.0481
0.1	0.0423	0.185	0.356	3.72	0.113	0.0214
0.05	0.0149	0.106	0.143	1.74	0.0797	0.0178

However, a detailed study [3] has recently suggested a nearly linear relationship between the bubble volume and Q / Q_{crit} value, with a factor of about 3 increase of

bubble volume from Q / Q_{crit} ~ 0 to 1. If compared with the constant gas flow cases of Q / Q_{crit} ~ 0.1 (to ensure small bubble size), the pulsating gas flow throughput Q in Table 11 may not seem unreasonably low with the benefit of substantially reduced bubble size (especially for smaller micro-needles).

Considering the data in Table 11 represent the throughput values for minimum feasible bubble size, the bubble throughput Q is expected to increase with longer $\Delta\tau$ or higher U_a if larger bubbles are acceptable. However, care should be taken when operating with relatively high U_a as severely deformed bubbles may break up into uncontrollable pieces after detachment, as indicated by the present simulations when *Re* and *We* are increased to large values. Such situations of bubble break-up require resource-demanding full three-dimensional simulations, which would be beyond the scope of the present exploration with axisymmetric case simulations.

4. Concludding Remarks

The feasibility of generating axisymmetric bubbles of sub-millimeter diameters with rectangular-wave pulsating gas flows is demonstrated through computational results using a previously verified OpenFOAM® VOF model. In view of the computed cases for air bubbles in water, the key enabling factor appears to be the pulse amplitude which, when sufficiently high, can reduce the normalized bubble sizes to d / D < 2 by shrinking the pulse width $\Delta\tau$ to its minimum value. Even with thin-wall needles, liquid wetting behavior on the needle wall can have a significant effect, similar to that

revealed in previous studies for constant gas flow cases [3, 10] (i.e., liquids with contact angle ~45^{o} or less are favorable).

When extending the study to the effects of liquid viscosity and surface tension, primary trends for bubble size reduction with pulsating gas flow are revealed in terms of the familiar fluid dynamics parameters such as Reynolds number *Re* and Weber number *We* (as shown in Fig. 9). This implies that the reduction of bubble size can mostly be enabled by increasing the pulse amplitude and reducing the liquid viscosity, for a given needle size. Although using smaller needles can help generate smaller bubbles, it also results in shrinking parameter windows and increasing sensitivity to parameter variations. The effects of surface tension on reducing bubble size appear mixed: it generally helps when the liquid viscosity is low, but may hinder when viscosity is relatively high.

The complexity of surface tension effects may be understood by examining the evolving meniscus shape around the neck region, in view of the fact that the local free surface takes a shape similar to that of a pendular bridge with two opposing principal curvatures. While the capillary force due to the curvature of the neck radius tries to shrink the neck for pinch-off, that of the meridional curvature acts in just the opposite direction, to prevent the neck pinch-off. Which side wins the delicate competition depends on the detailed dynamics of the evolving meniscus shape at specific transient moments.

For now, the possibility of reducing bubble size to $d < 2\,D$ with pulsating gas flow revealed in the present work still remains at the theoretical level. Most of the

experimental results with pulsating gas flows in the literature showed $d > 10\ D$, e.g., $d >$ 0.4 mm with $D \sim 0.02$ mm by Najafi et al. [4], $d > 0.65$ mm with $D \sim 0.06$ mm by Song et al. [8], while Shirota et al. [5] could obtain microbubbles of $d \sim 3\ D$ with a $D = 0.18$ mm orifice. The difficulties in producing microbubbles of theoretically predicted $d < 2\ D$ in experiments could be a consequence of the lack of understanding of the narrowing parameter windows for orifices of $D << 1$ mm, in terms of *Re* and *We*, revealed in the present work. Hopefully, the computational results presented here can provide insightful guidance for future endeavor to generate minimal microbubbles in laboratories. The present pulsating gas flow results may also help establish the theoretical basis for accurately controlled bubble-on-demand applications.

ACKNOWLEDGMENT

...

FUNDING

None

NOMENCLATURE

Ca	capillary number
d	bubble diameter (mm)
D	orifice diameter (mm)
F_b	impulse force in units of buoyancy force
F_σ	impulse force in units of capillary force
g	acceleration of gravity
Oh	Ohnesorge number
Q	gas volumetric flowrate (mm^3/s or $\mu L/s$)
Re	Reynolds number
t_σ	capillary timescale
U_a	rectangular-wave pulse amplitude of gas inlet velocity (m/s)
V	bubble volume (mm^3 or μL)
We	Weber number
ΔT	pulse cycle period
$\Delta\tau$	rectangular-wave pulse width (ms)
μ	liquid dynamic viscosity (cp)
θ	three-phase contact angle (deg)

ρ	liquid density (kg m^{-3})
σ	surface tension (kg s^{-2})
τ	bubble detachment time (ms)

REFERENCES

[1] Clift, R., Grace, J. R., and Weber, M. E., 1978, *Bubbles, Drops, and Particles,* Academic Press Inc., New York, Chap. 12

[2] Oguz, H. N., and Prosperetti, A., 1993, "Dynamics of bubble growth and detachment from a needle," J. Fluid Mech., **257**, pp. 111-145.

[3] Feng, J. Q., 2026, "A computational study of bubble formation from an orifice submerge in liquid with constant gas flow," J. Fluids Eng., **148(1)**, p. 011404.

[4] Najafi, A. S., Xu, Z., and Masliyah, J., 2008, "Single micro-bubble generation by pressure pulse technique," Chem. Eng. Sci., **63,** pp. 1779-1787.

[5] Shirota, M., Sanada, T., Sato, A., and Watanabe, M., 2008, "Formation of a submillimeter bubble from an orifice using pulsed acoustic pressure waves in gas phase," Phys. Fluids, **20**, p. 043301.

[6] Brittle, S., Desai, P., Ng, W. C., Dunbar, A., Howell R., Tesai, V., and Zimmerman, W. B., 2015, "Minimising microbubble size through oscillation frequency control," Chem. Eng. Res. Des., **104**, pp. 257-366.

[7] Song, A., Ji, Y., Li, C., and Cao, Y., 2021, "Modeling and validation of the momentum force for bubble formation from submerged orifices with an oscillatory air supply," Chem. Eng. Sci., **233**, p. 116387.

[8] Song, A., Zhao, S. Li, C., and Cao, Y., 2022, "A quantitative study on the decreased diameter of bubbles generated from a submerged orifice with an oscillatory air supply," Ind., Eng. Chem. Res., **61(8)**, pp. 3113-3122.

[9] Chen, Z., Yu, J., Fan, W., Xi, J., Huo, Y., Bandulasena, H. C. H. and Huo, M., 2025, "Minimising the bubble size through fluidic control of formation at a submerged orifice: The role of oscillatory inflow," Water Res., **277**, p. 123309.

[10] Gerlach, D., Biswas, G., Durst, F., and Kolobraric, V., 2005, "Quasi-static bubble formation on submerged orifices," Int. J. Heat Mass Transfer, **48**, pp. 425-438.

[11] Ohta, M., Kiluchi, D., Yoshida, Y., and Sussman, M., 2011, "Robust numerical analysis of the dynamics bubble formation process in a viscous liquid," Int. J. Multiphase Flow, **37(9)**, pp. 1059-1071.

[12] Roenby, J., Bredmose, H., and Jasak, H., 2016, "A computational method for sharp interface advection," Roy. Soc. Open Sci., **3**, 160405.

[13] Gamet, L., Scala, M., Roenby, J., Scheufler, H., and Pierson, J.-L., 2020, "Validation of volume-of-fluid OpenFOAM® isoAdvector solvers using single bubble benchmarks," Comput. Fluids, **213**, 104722.

[14] Mulbah, C., Kang, C., Mao, N., Zhang, W., Shaikh, A. R., and Teng, S., 2022, "A review of VOF methods for simulating bubble dynamics," Prog. Nucl. Energy, **154**, 104478.

[15] Feng, J. Q., 2017, "A computational study of high-speed microdroplet impact onto a smooth solid surface," J. Appl. Fluid Mech., **10(1)**, pp. 243-256.

[16] Helsby, F. W., and Tuson, K. R., 1955, "Behaviour of air bubbles in aqueous solutions," Research, **8**, p. 270.

[17] Fritz, W., 1935, "Berechnung des maximale volume dampfblasen (Calculation of maximum volume vapor bubbles)," Phys. Z., **36**, pp. 379-384.

[18] Van Krevelen, D., and Hoftijzer, P., 1950, "Studies of gas-bubble formation: calculation of interfacial area in bubble contractors," Chem. Eng. Prog., **46**, pp. 29-35.

[19] Kumar, R., and Kuloor, N. R., 1970, "The formation of bubbles and drops," Adv. Chem. Engng., **8**, pp. 256-368.

[20] Bari, S. D., and Robinson, A. J., 2013, "Experimental study of gas injected bubble growth from submerged orifices," Exp. Therm. Fluid Sci., **44**, pp. 124-137